EARTHQUAKE HAZARD AND PREDICTION IN NW MEXICO AND CALIFORNIA/MEXICO BORDER

Michael Reichle and James N. Brune

University of California, San Diego
Institute of Geophysics and Planetary Physics
Scripps Institution of Oceanography
La Jolla, California 92093

USGS CONTRACT NO. 14-08-0001-19163
Supported by the EARTHQUAKE HAZARDS REDUCTION PROGRAM

OPEN-FILE NO. 82-62

U.S. Geological Survey
OPEN FILE REPORT

Introduction

During the past contract year, we have concentrated on reducing and analyzing digital and analog data collected following the 15 October 1979 Mexicali and the 9 June 1980 Victoria earthquakes. Research is being directed toward an understanding of the differences and similarities of these two events. The most obvious differences were in the surface ruptures. The 1979 Mexicali event produced a surface rupture 30 km long, with a maximum displacement of almost 80 cm. The Victoria event, while almost of equal magnitude, produced no extended surface rupture; short segments with both small left and right lateral slip were observed, but these were perhaps associated with local ground failure. One interesting similarity between the two sequences is that in each case the rupture appears to have begun at the southern end of the zone, more or less in mid-transform fault, and propagated toward a nearby spreading center segment. Also, in each event, most aftershocks occurred in the vicinity of the spreading center, as a swarm-like sequence, while the main-event rupture zone was relatively quiescent. The physical causes of these similarities and differences, and why both sequences are different than the more accepted definition of an aftershock sequence, may become clearer as we analyze both the local and teleseismic data from each event. Preliminary analyses are discussed below.

We also include a preliminary report on analyses of teleseismic data from the 29 November 1978 Oaxaca and the 14 March 1979 Petatlan earthquakes. The SRO LP recordings of both events are quite similar, suggesting similar rupture processes. The results are compared with

that of a smaller event which occurred on 26 January 1979 only about 100 km away from the subsequent Petatlan event. This work is essentially completed. By the end of summer, all loose ends should be tied up and the results ready for publication.

Research will continue under contract number USGS USDI 14-08-0001-19852.

The 15 October 1979 Mexicali Earthquake

Within 6 hours after the 15 October 1979 (M_L = 6.4) Mexicali earthquake, portable seismic recorders (drum and digital) were installed along the Imperial fault south of the international border. These instruments, along with the stations of CICESE's permanent Cerro Prieto network, could insure more accurate location of any aftershocks which would occur in Mexico. After preliminary lcoations, information from Cal Tech and a reconnaissance of the Imperial fault showed that most activity was north of the border, so some of the digital equipment was moved north of the border for other experiments. During the early part of the experiment, the digital equipment was set with fairly low gains. Thus, we should be able to locate many of the aftershocks which occurred during that time, when the higher gain Southern California stations were too noisy due to the many smaller aftershocks.

Over a time span of 30 days, a total of 10 stations were occupied by digital recorders operated by CICESE and IGPP, resulting in over 100 full cassettes of aftershock data. The contents of all cassettes have been transferred to computer-compatible tape and catalogued.

Aftershocks recorded by the portable array are being read and located by CICESE. A preliminary map showing the epicenters located in Mexico is provided in Figure 2. Several special studies involving source mechanisms and parameters and local structure are being conducted jointly by CICESE and IGPP. S-wave spectra have been computed for aftershocks closely following the main event. The stress drops determined therefrom range from 1 to 200 bars; this is too small a sampling of data, however, to state flatly at this time that there are no higher stress events involved. Aftershocks occurring later in the sequence will be analyzed shortly. Comparisons of the presently available stress drop data from the Mexicali earthquake aftershocks with those from the 1980 Victoria earthquake aftershocks (Figure 1). offer no indication of any differences in the stress regimes. However, comparison of these aftershock data with data from the 1978 Victoria swarm shows a clear difference, with stress drops (and moments) forthe 1978 swarm extending to much higher values, up to 1 kilobar, for approximately the same source dimension interval ($r \sim 0.1$ to 1.0 km). These remarkably high stress drop events may suggest a high stress regime prior to the 1980 earthquake, which may be considered premonitory to the earthquake. We will examine this possibility in detail.

In a study being performed by Dr. Krishna Singh (on sabbatical leave at IGPP from the Universidad Nacional Autonoma de Mexico in Mexico City), several aftershocks in the range $3.0 \lesssim M_L \lesssim 3.5$, recorded at 3 or more digital stations along the Imperial fault ($6 \lesssim R \lesssim 50$ km) have been selected to study seismic attenuation with distance. The objective of the study is to find a layered crustal structure with a Q distribution

with depth which best fits the observed data.

Understanding seismic attenuation in the Imperial Valley is an important step toward assessing seismic hazard in this region through better strong motion modelling and prediction.

The 9 June 1980 Victoria Earthquake

On 9 June 1980, at 03:28:20 (GMT), an earthquake of magnitude 6.2 (M_L) occurred in the Mexicali Valley, Northern Baja California, Mexico. The instrumental epicenter was located 11 km southeast of the town of Guadalupe Victoria. Four hours after the main event, the first of a portable array of 7 analog and 12 digital seismic event recorders, from both CICESE and IGPP (UCSD), began recording the aftershock activity.

The last recorder was removed from the region on 5 August 1980, following the accumulation of over 50 smoked-paper records and 60 digital cassettes containing aftershock data. The contents of all cassettes have been transferred to computer-compatible tape and time corrections have been determined for all stations. All usable signals have been edited from the computer-compatible tapes and archived. A convenient index to this catalogue of signals is being prepared.

Investigators at CICESE have located many of the aftershocks of the Victoria earthquake. They are clustered principally on a segment of the Cerro Prieto fault close to the two communities, Victoria and Pescaderos, which experienced the greatest damage from the mainshock. A number of events are also found scattered throughout the area between the southern end of the Imperial fault and the northern end

of the Cerro Prieto fault. The instrumentally determined epicenter of the mainshock (based on initial P arrivals at nearby USGS and Mexican stations) is on the Cerro Prieto fault, but is approximately 15 km southeast of the region of aftershocks and major damage. A similar phenomenon characterized the 15 October 1979 event on the Imperial fault (Chavez *et al.*, 1981).

Location of the aftershocks of this event continues to be pursued at CICESE, in addition to focal mechanism studies and a comparison of this event with previous events on the same fault system. At IGPP, S-wave spectra are being computed from some of the largest aftershocks.

An important aspect of the Victoria mainshock is the strong motion record obtained at a station in the town of Victoria. Vertical accelerations there exceeded 1g in both the positive and negative directions for several cycles, and the horizontal acceleration reached .85g. Figure 9 shows a comparison of the response spectrum for the Victoria event with the highest response spectrum for the 1979 Imperial Valley event. Understanding this record will be crucial to understanding the mechanism and hazard from earthquake strong motion. A paper on this recording will be given at the forthcoming meeting of the Seismological Society of America in Berkeley during March, as will papers on the locations and mechanisms of the aftershocks and the geological effects and damage distribution of the main event.

Soon after the Victoria earthquake, the region was inspected carefully from the air and on the ground by observers from both IGPP and CICESE. Many fissures and sand blows and other surface manifestations

were seen striking roughly perpendicular to the strike of the Cerro Prieto fault system. However, no surface features paralleling the fault system were detected. This contrasts sharply with observations of surface faulting on the Imperial fault following the 15 October 1979 Mexicali event. Greater detail on these observations is contained in the abstract (Suarez *et al.*, 1981), as well as a report on "Strain and displacement measurements for the June 8, 1980 Victoria, Mexico earthquake" (Chavez *et al.*, 1981). This report summarizes results from a microgeodetic network installed 22 km southeast of Victoria one month before the earthquake and resurveyed immediately thereafter.

Regional and Local Seismicity Associated with the 1978 Victoria Swarm and the 1980 Victoria Earthquake

In order to have a general picture of the seismicity in the Victoria area, we have plotted cumulative number of events, taken from the Cal Tech catalogue, vs. time. Figure 2 shows the cumulative plot for a 30 km radius around the central Cerro Prieto fault (circled area in insert) from 1971 - 1980. The seismicity was relatively constant between 1971 and 1978 until the Victoria swarm occurred in March, 1978, with very high seismicity for a couple of weeks. From the 1978 swarm until the 1980 Victoria earthquake, the indicated level of seismicity was higher, however this result must be viewed with caution since during this time the Southern California array had an increased sensitivity for Mexican earthquakes, compared to earlier. In 1980 the seismicity greatly increased as a result of aftershocks of the Victoria earthquake. It is tempting to speculate that the 1978 Victoria swarm was linked, as a premonitory event, to the 1980 Victoria earthquake,

since the swarm and the earthquake occurred in essentially the same area. As noted above, the Victoria swarm was characterized by some very high stress drop events which may suggest a local stress concentration which finally broke in the 1980 earthquake.

If we consider a moment vs. time plot of this area, we find that it is completely dominated by the 1934 and 1980 large earthquakes in this region. The moment for the 1980 earthquake, estimated from the surface wave magnitude 6.4 is about 7×10^{25} dyne-cm. (The corresponding moment for the 15 October 1979 Imperial Valley earthquake, $M_s \sim 6.9$, is 2.5×10^{26} dyne-cm, $\sim$4 times greater). The 1934 earthquake with $M_s \sim 7$ (Gutenberg and Richter) had a moment somewhat larger than the 1979 Imperial Valley earthquake, i.e., $\sim$5 times greater than the Victoria earthquake. In order to compare the moments of earthquakes with expected slip along the Cerro Prieto fault we have constructed the approximate moment release diagram in Figure 8. We have averaged the slip based on moment over a 40 km segment for each earthquake as a rough approximation, even though the exact rupture zone of each earthquake is not known. The moments are based on the surface wave magnitudes shown in this figure. As can be seen, the northern part of the Cerro Prieto fault has not released enough moment in the last 50 years to keep up with the estimated plate motion of 6 cm/yr, and is considerably behind the southern part of the Cerro Prieto fault and the southern part of the Imperial fault. This suggests that there is still probably considerable strain energy stored along the northern part of Cerro Prieto fault and we may expect continued high seismicity and perhaps another moderate sized earthquake.

Research During 1981/1982

During the present contract year, we hope to complete our studies of the Mexicali and Victoria mainshocks and aftershocks. We will help CICESE in installation of the telemetering seismic array and with analysis of the data as it begins to be received.

At the same time, we plan to begin to monitor the seismic gap along the southern Cerro Prieto fault in the vicinity of and to the south of the 1980 Victoria event. This region is not closely covered by either the CICESE Cerro Prieto local or the Northern Baja regional networks. To fill in, then, we plan to install three portable digital seismic recorders in this region this summer. The main purpose of the array will be to provide location control for events in the central and southern Mexicali Valley with stations to the south. Also, changes in seismicity levels and spectral parameters, which may be precursory to a larger event, will be more easily detectable with a more local array, than with the further stations of a regional array.

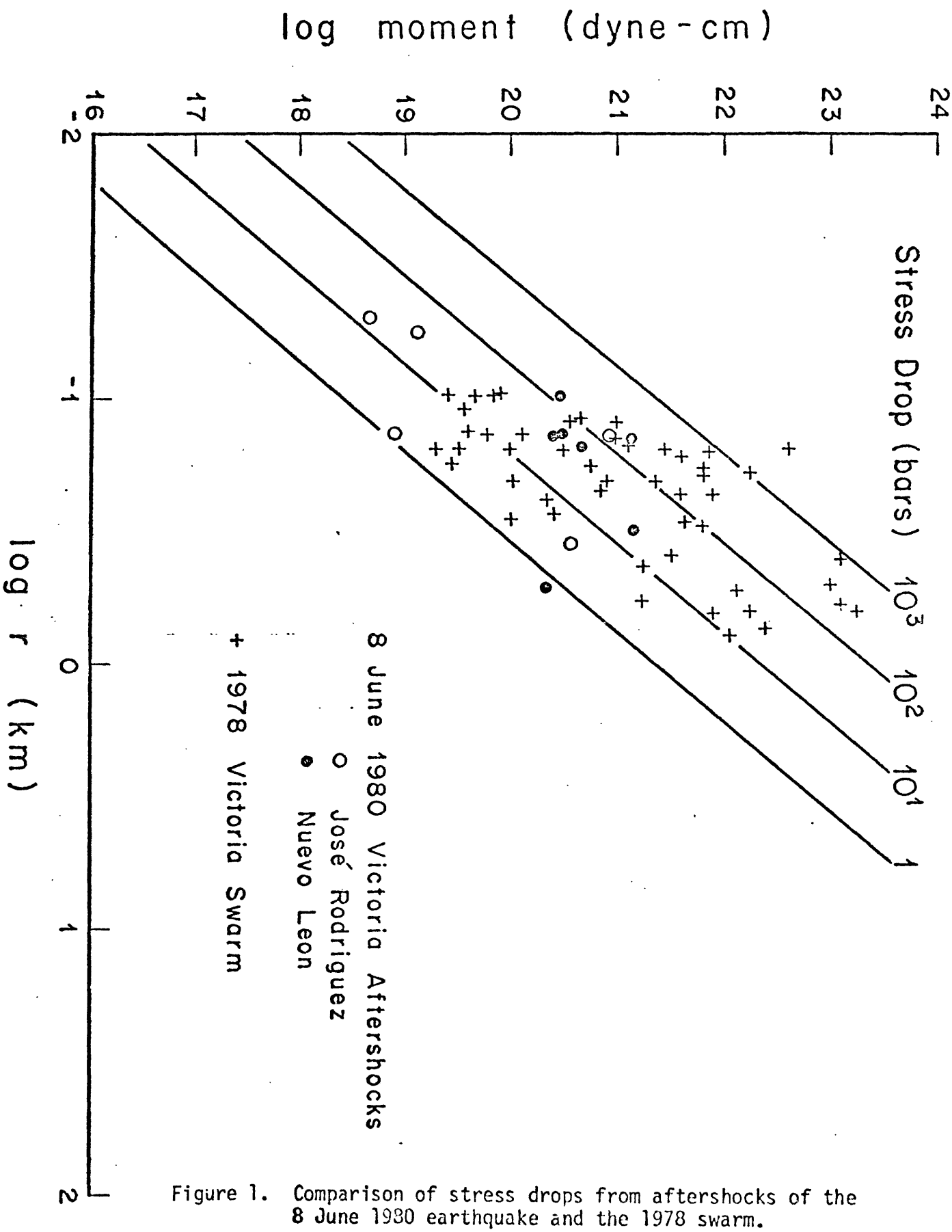

Figure 1. Comparison of stress drops from aftershocks of the 8 June 1980 earthquake and the 1978 swarm.

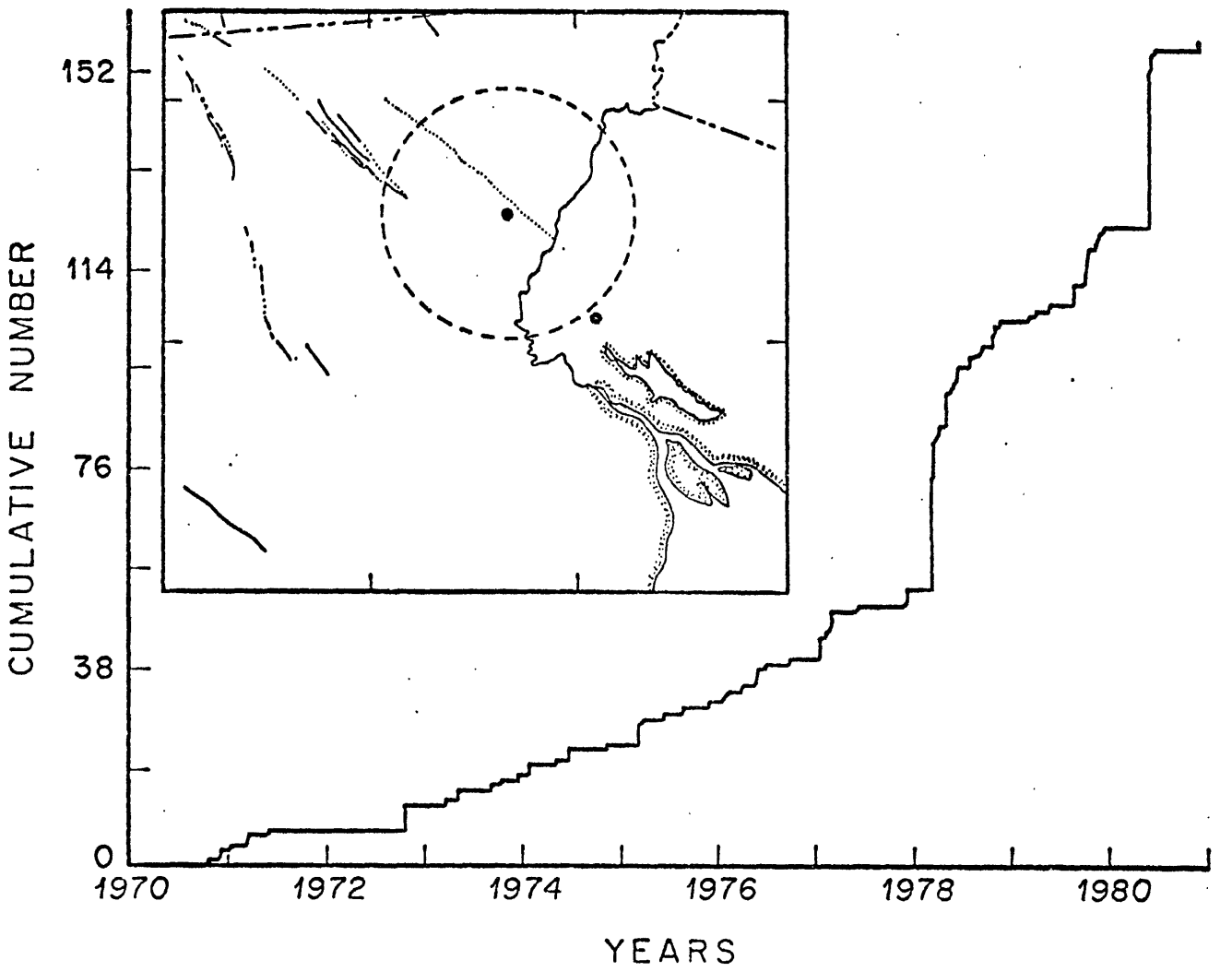

Figure 2. Number of earthquakes (cumulative) since 1971 in circled area surrounding central portion of Cerro Prieto fault.

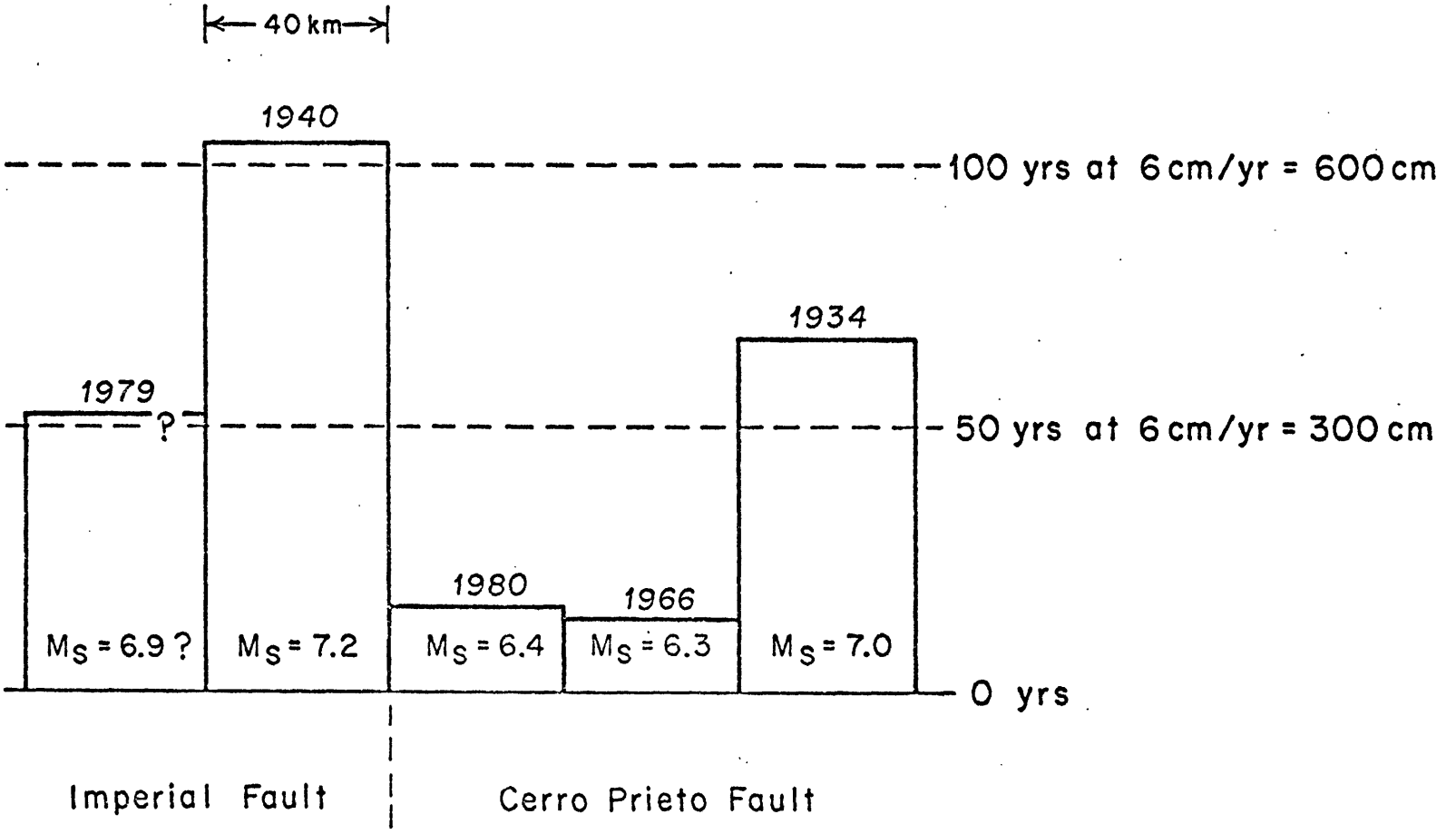

Figure 3. Diagram of historical moment release on the Imperial and Cerro Prieto faults. Bar heights represent average slip based on moment computed from the surface wave magnitudes shown, assuming a 40 km rupture length and 10 km depth for each earthquake.

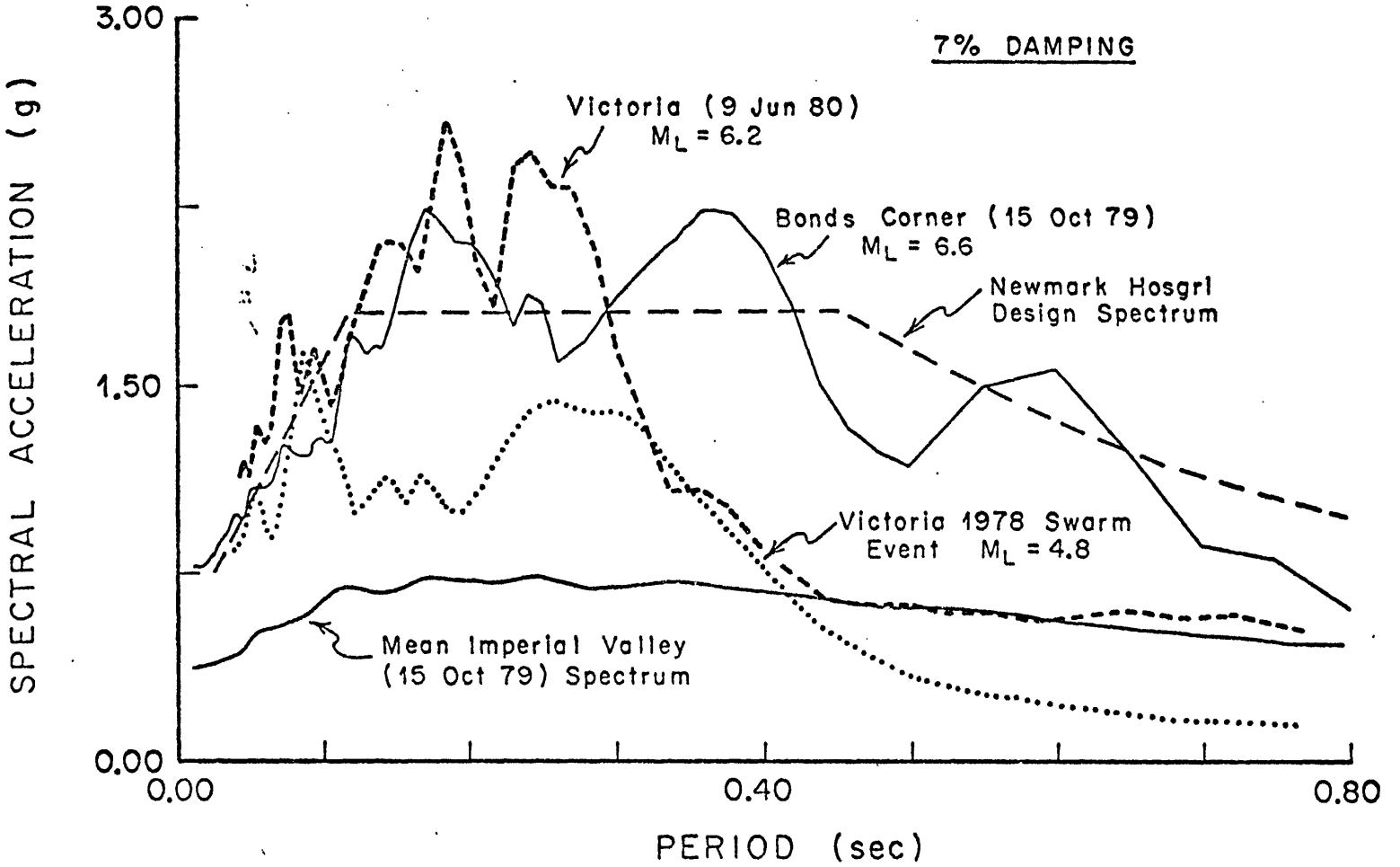

Figure 4. Horizontal acceleration response spectra from the 9 June 1980 Victoria earthquake (recorded at Victoria), the 15 October 1979 Imperial Valley earthquake (recorded at Bond's Corner), an earthquake from the 1978 Victoria swarm (recorded at Victoria), plus the mean Imperial Valley spectrum and the Newmark Hosgri Design spectrum (for the Diablo Canyon nuclear power plant).

APPENDIX A

We have studied waveform data from the large 29 November 1978 Oaxaca ($M_S \sim 7.8$) and 14 March 1979 Petatlan ($M_S \sim 7.6$) earthquakes with a goal of extracting both kinematic and dynamic fault parameters. We have relied heavily on data from the Seismic Research Observatory (SRO) and the International Deployment of Accelerometers (IDA) networks. WWSSN recordings have been used only for first motion data since so many of these records were clipped or driven into nonlinear response region by the magnitude of the events. The waveforms for the two events are nearly identical; we shall discuss the Oaxaca event in detail and many of the conclusions are applicable to both events.

We have modeled the recorded SRO data using the WKBJ asymptotic algorithm of Chapman (1978). Because this approximation is invalid in the vicinity of a large velocity discontinuity and low velocity zone such as the core-mantle boundary, we have restricted our data set to epicentral distances less than 85°. In addition, substantial lateral heterogeneities at depths less than 800 km prevented the use of data recorded within an epicentral distance of 39°. In the initial stages of the modeling procedure we made use of P, PP and PPP phases formed by contributions from the up- and down-going P waves and up-going S waves at the source. Use of the higher-order multiples, of course, allowed us to consider epicentral ranges well in excess of 85° since the turning points of these phases all occurred in the lower mantle. Attenuation was modeled with a causal Q operator (Futterman, 1962) with a t* of 1.

Initial estimates of the moments of the events were obtained

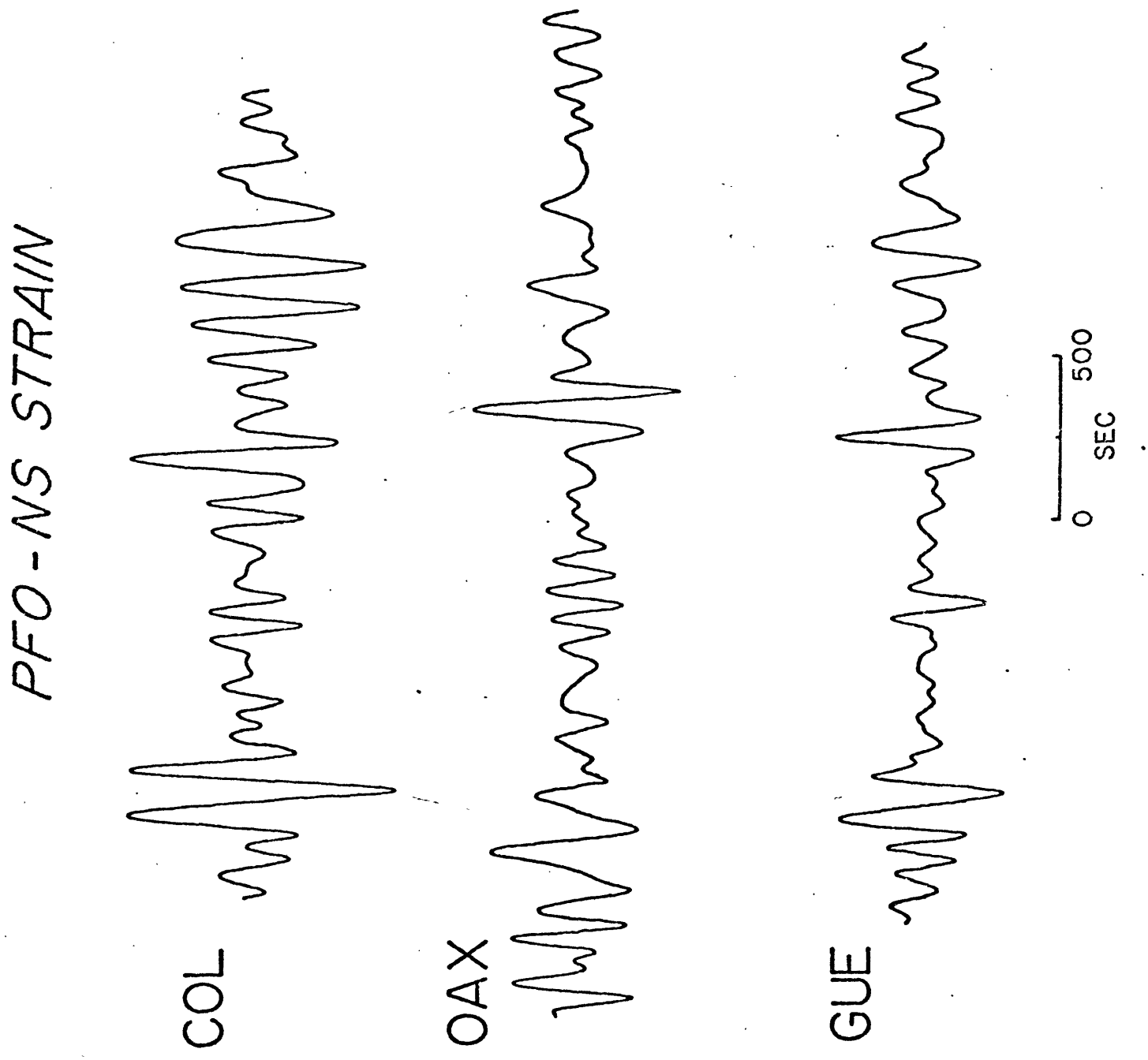

Figure 1. Piñon Flat Observatory north-south laser strainmeter recordings of mantle Rayleigh waves from three Mexican earthquakes: Colima, Oaxaca and Petatlan, Guerrero.

from the Piñon Flat laser strainmeter. Figure 1 illustrates recordings of north-south strain for long period mantle surface waves from the 1973 Colima event ($M_s \simeq 7.5$) compared to the Oaxaca and Petatlan (labeled GUE) recordings. Without taking into account possible small differences in the source mechanisms or focusing due to rupture propagation, the seismic moment of the Oaxaca earthquake, estimated from a direct comparison of amplitudes, is $1.5 - 3 \times 10^{27}$ dyne-cm while the moment of the Petatlan event is smaller, $1.5 - 2 \times 10^{27}$ dyne-cm. Both events are smaller than the Colima event which Reyes *et al.* (1979) estimated to have a moment of $3 \pm 1 \times 10^{27}$ dyne-cm.

The fault plane solutions on Figure 2 provide control only on the auxiliary plane. The slip vector has a dip of about 10° - 12° and a strike, in the case of Oaxaca, of 035 and, for Petatlan, 026 to 042. These slip vectors are in good agreement with estimates of motion between the America and Cocos plates (Minster and Jordan, 1978).

The compressional wave data used for body wave analyses are shown in Figure 3. The waveforms are plotted at their correct azimuths with respect to the source and the approximate strike of the fault is plotted at the center of the circle. Clearly ZOBO is near a node and the first motion is slightly up. Figure 4 illustrates the effects of dip of the fault plane for a source depth of 25 km and a purely thrust source mechanism. The "best fit" for this set of parameters occurs for a shallow dip between 6° and 10°. The experiment was repeated for a source depth of 15 km and we concluded that the long period, narrow-band SRO data prevented clear differentiation between the two source depths. The effect of the length of the source time function for Oaxaca is outlined in Figure 5. Four compressional waves are shown with their amplitudes

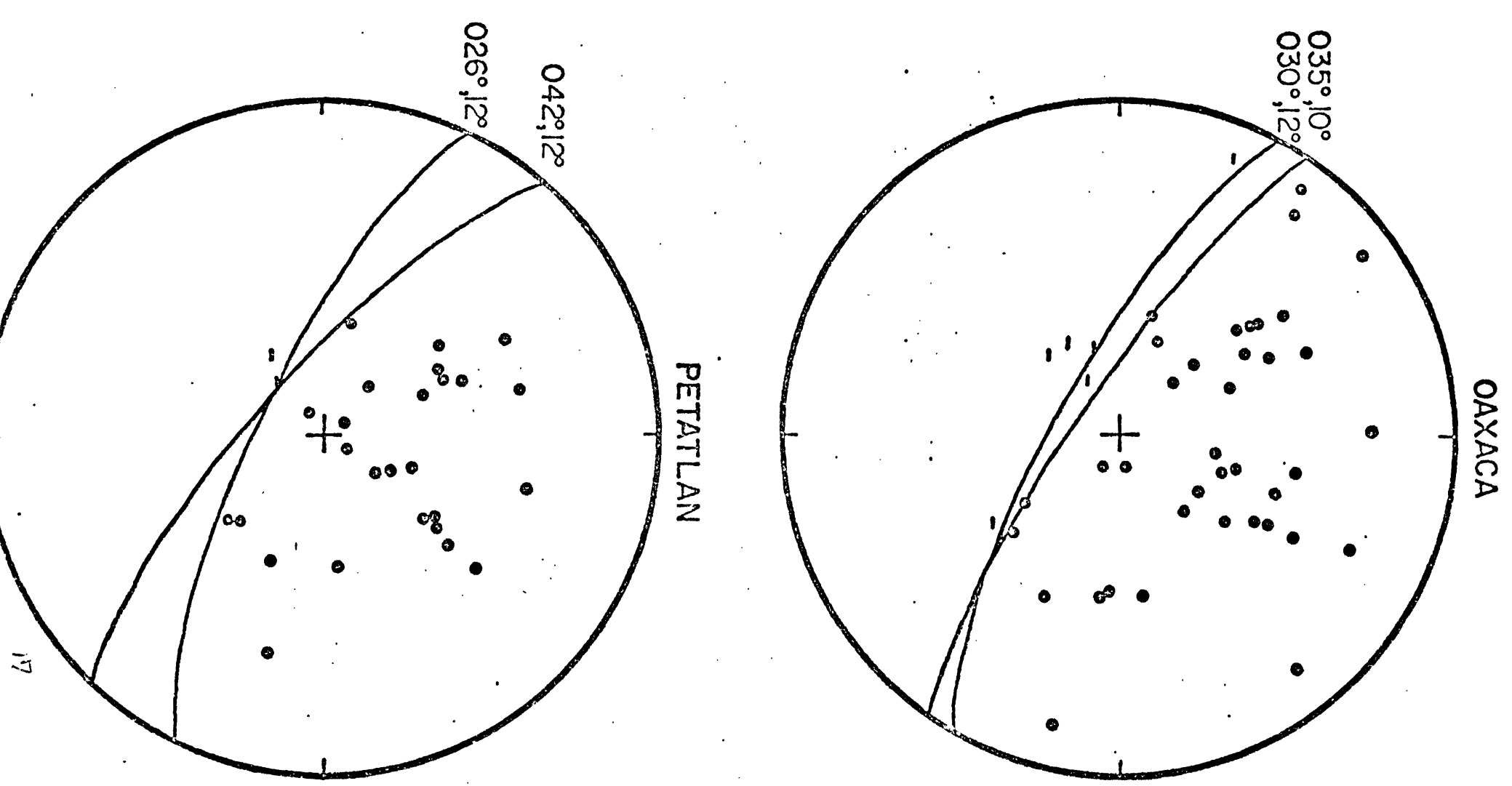

Figure 2. Fault plane solutions for the Oaxaca and Petatlan events using available WWSSN and SRO data. Dots represent compressions while dashes denote refractions.

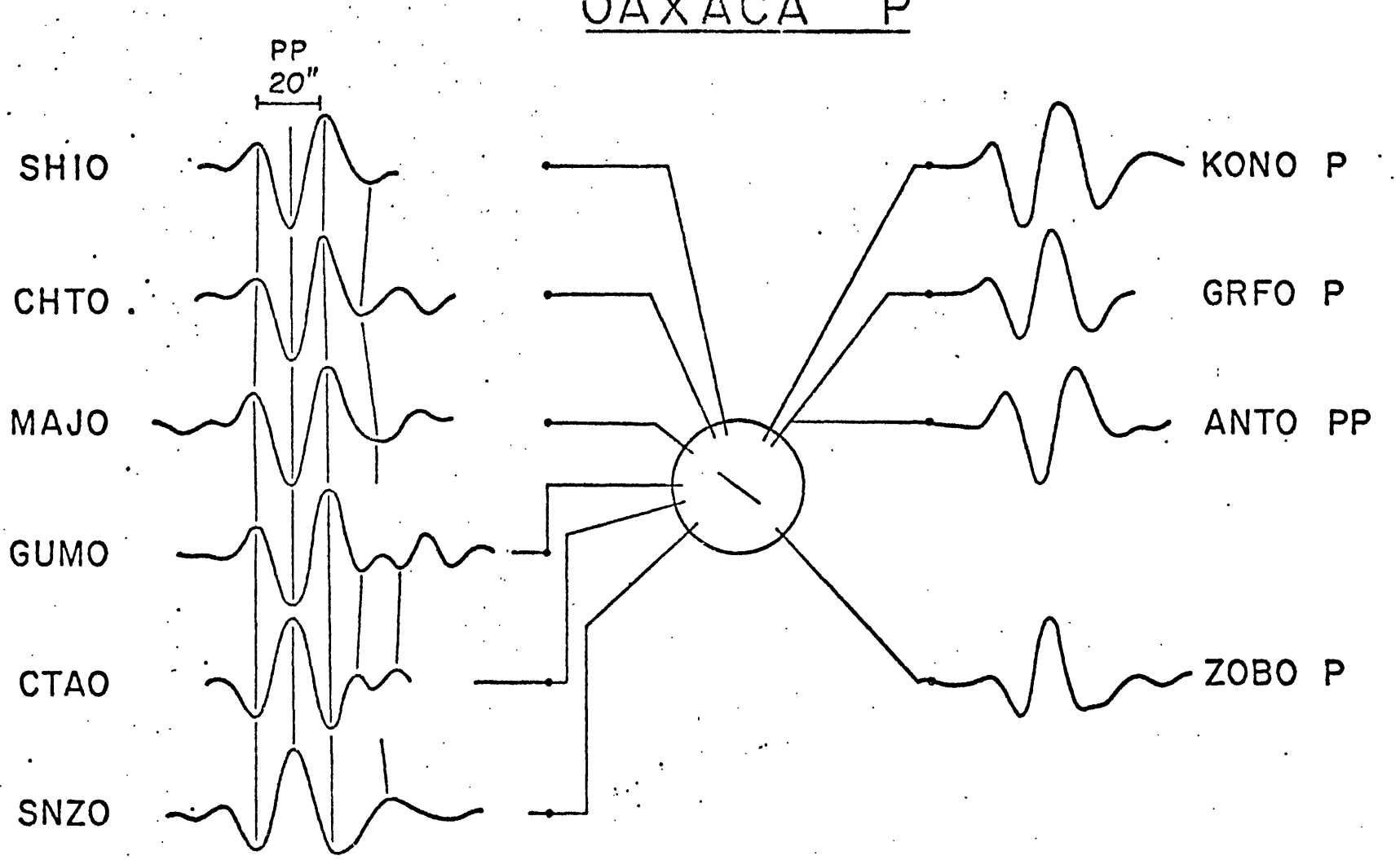

Figure 3. Compressional wave recordings used on the analysis of the Oaxaca event. Note ZOBO is near a node. The line at the center of the circle represents an approximate fault strike. The apparent frequency content of PP is independent of azimuth as illustrated by the vertical lines connecting the peaks and troughs.

in counts and synthetics for different length triangular source time functions are plotted beneath the data. The annotation on each seismogram is the theoretical amplitude for a moment of 3×10^{27} dyne-cm. A total function length of 16 - 20 sec is generally consistent with the data set.

The compressional wave data provided no substantial control on the strike of the fault plane. In an attempt to resolve this ambiguity, the excitation of the fundamental Rayleigh mode was examined for orbits R2 and R3 recorded by the IDA network. These data are plotted in Figure 6 with predicted amplitudes for the fault parameters shown. The data are consistent with a fault plane essentially parallel with the strike of the trench axis at the two epicenters. We also note the moment estimates from the SRO body wave data and the IDA surface wave data are consistent with an amplitude of $3 - 3.5 \times 10^{27}$ dyne-cm for the Oaxaca event and $1.5 - 2 \times 10^{27}$ dyne-cm for the Petatlan earthquake.

We have examined the rotated SH components at the various SRO stations in order to gain additional control on the source mechanism. The data used are summarized in Figure 7 at their correct azimuths. Again both S and SS pulses have been used and the amplitudes, in counts, are shown with each seismogram. Stations in the western Pacific and Asia clearly show a dependence of the phase on the azimuth, particularly late in the S-wave pulse.

Various source time function lengths and t* values were used to generate the synthetic seismograms in Figure 8 which are compared to data at GUMO and ZOBO. For GUMO, the best phase fit is achieved for a t* of 10 and a source time function length of 10 seconds or a t* of 4 and a length of 16 sec. For ZOBO, on the other hand, a source time function

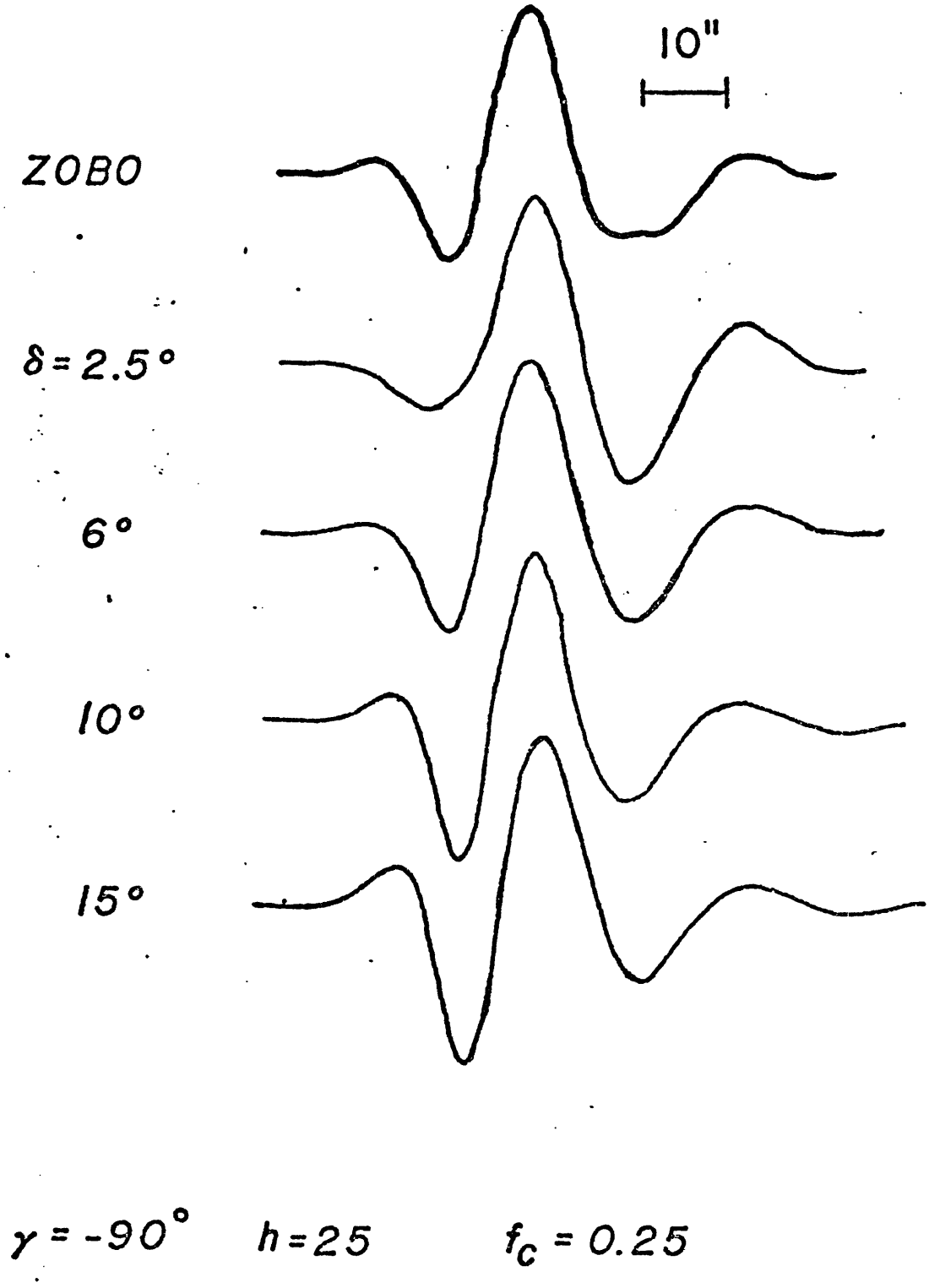

Figure 4. The effect of ranging the fault plane dip angle upon the predicted phase at ZOBO. A shallow dip between 6 and 10 degrees provides a good fit to the data.

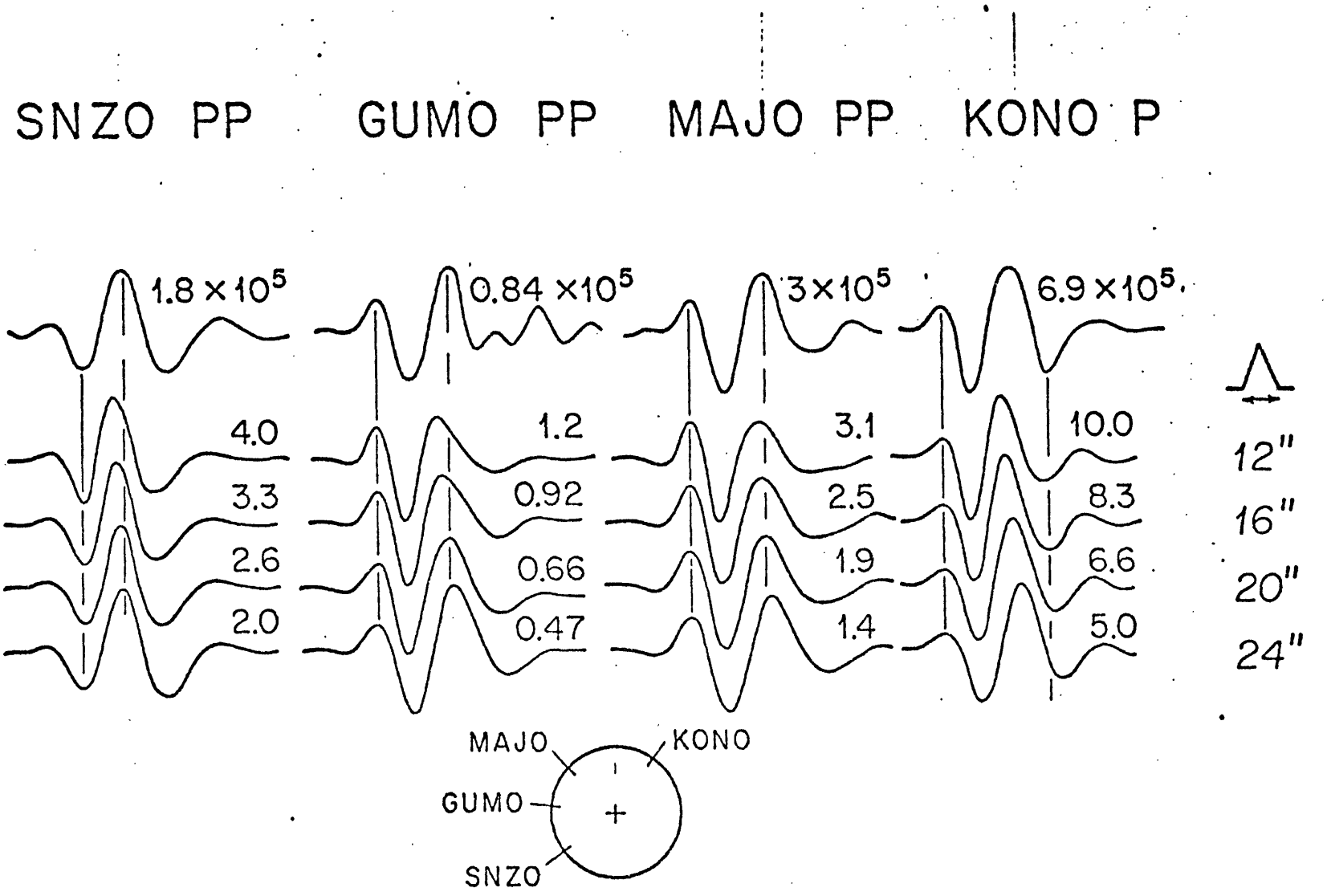

Figure 5. The effect of the length of the source time function on the predicted seismograms. A total length of 16 - 20 seconds provides the overall best phase and amplitude fit to the data. The amplitudes presume a source moment of 3×10^{27} dyne-cm.

length of 24 seconds and a t* of 5 is preferred. We found that a single t*, source time function length could not be found which fit all the data; in effect, the source time function was found to be dependent on the source-receiver azimuth. Furthermore, the predicted amplitudes for the optimal source time function, t* combination at a given station always vastly exceeded the observations.

Amplitude studies of single events are unlikely to provide any real resolution for attenuation or t* in the SRO bandwidth. Figure 9 is a plot of the amplitude spectra of the Futterman Q operator for t* values of 3, 5 and 7. Clearly, the amplitude decrements inside the approximate bandwidth are much smaller than the variance in the data-synthetics residuals. We have used a t* of 3 for S-wave propagation and, as illustrated, we cannot expect a reasonable choice for attenuation to yield predicted amplitudes small enough to fit the data.

We have, finally, computed S-wave synthetics for a finite-sized fault plane. Figure 10 outlines the expected effects of propagation direction on the waveforms. The fault plane was taken to be vertical for illustration and sources were placed at coarsely spaced grid depths of 15, 40 and 65 km. Each frame plots the Green's function at the top and the Green's function convolved with the SRO impulse response at the bottom. Downdip propagation yields a minimum phase wavelet while updip propagation results in a maximum delay wavelet. The bilateral model gives rise to a mixed-delay wavelet.

Synthetic seismograms for the S-wave data are illustrated in Figure 11 for updip and downdip propagation on a fault plane dipping at 10° with an azimuth of 305°. The preferred model yielding the best phase fit involves downdip propagation and the predicted amplitudes

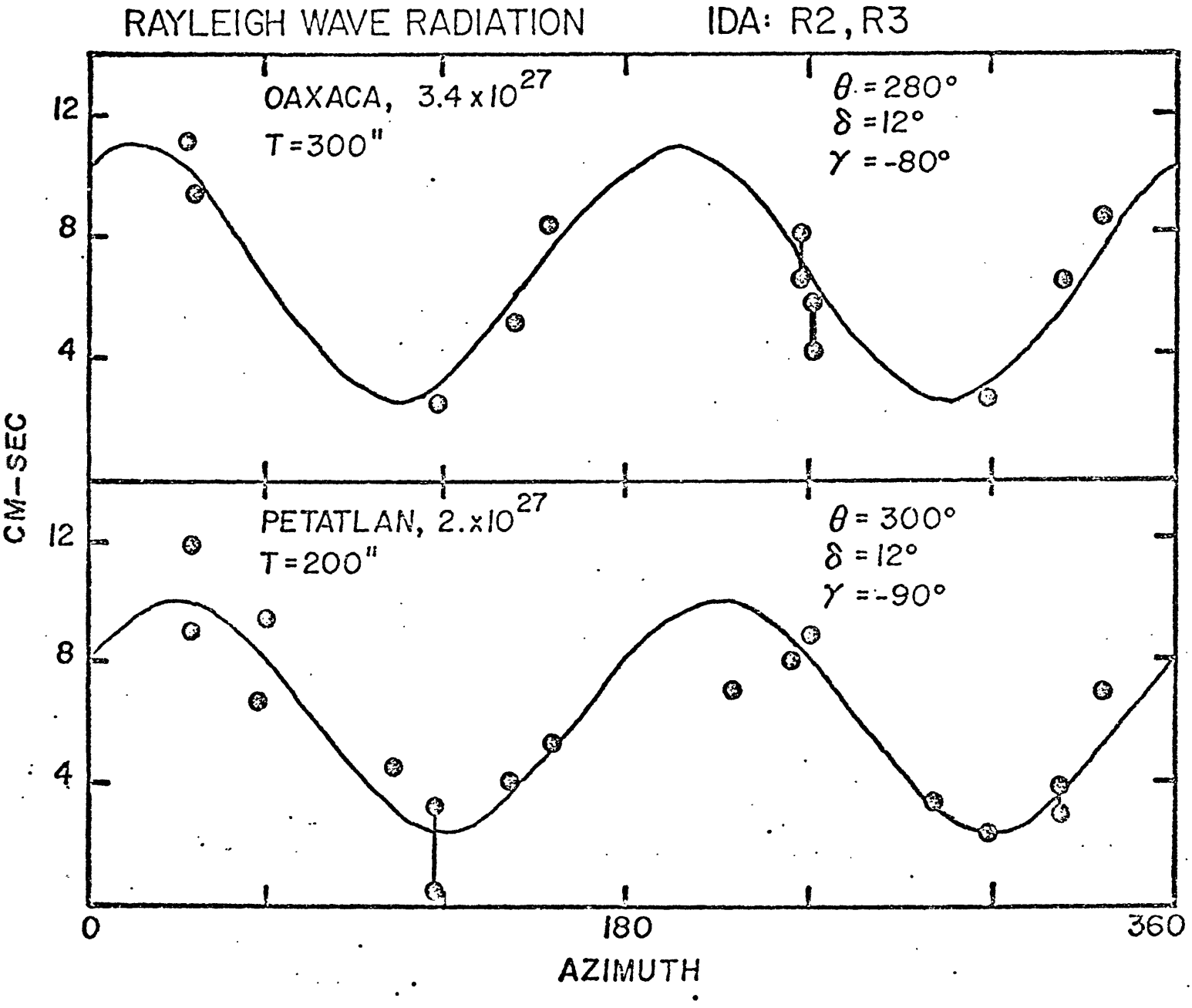

Figure 6. Surface wave excitation for the two events studied using the fundamental Rayleigh wave data from orbits R2 and R3 as recorded on the IDA network. The modeled amplitudes assumed the shallow thrust fault parameters shown and are consistent with the moments determined from the body wave studies.

are now consistent with the data. The predicted amplitudes assume a source moment of 3×10^{27} dyne-cm. The area of rupture used was 90 km along dip with bilateral rupture extending horizontally out to 30 km on each side. That is, the area of faulting is conssitent with the observed aftershock area if the rupture velocity is equal to the shear velocity of the medium (Singh *et al.*, 1980; Reyes *et al.*, 1978).

In the beginning of this study, we had expected that a point source approximation would be valid given the long periods and large wavelengths recorded by the SRO network. Acceptable synthetic seismograms could be produced, in fact, if the absolute amplitudes were ignored and the azimuthal dependence of the S-waves was overlooked. However, these data were so compelling we found the only acceptable fault model available to us involved a source with finite dimensions. The implications of this result are, of course, substantial. For example, automatic moment tensor retrieval algorithms which make use of S-wave propagation may be biased in an unknown direction by the assumption of an infinitesimal source model.

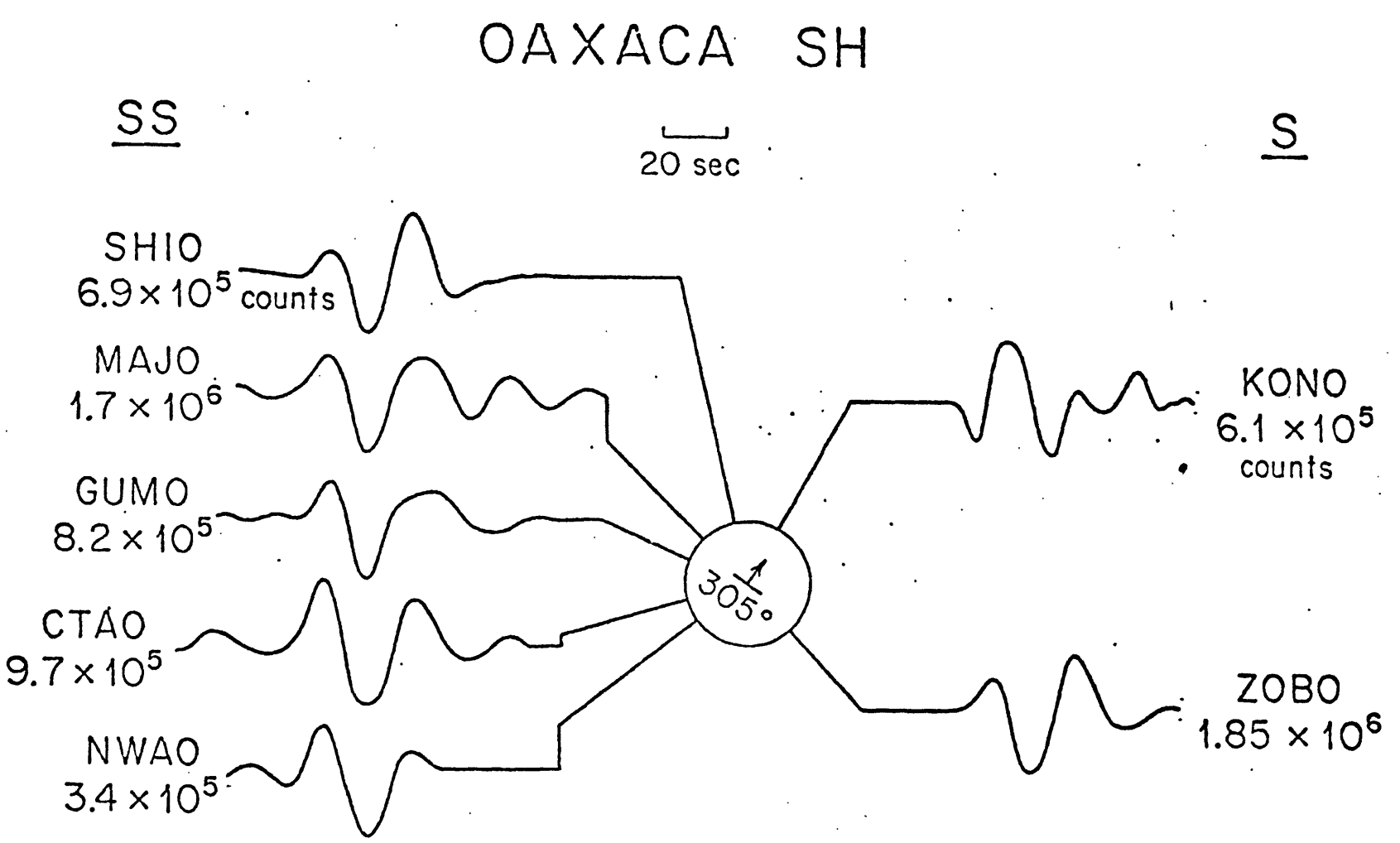

Figure 7. Tangential (SH) S and SS wave data used in this analysis. The data were obtained by an appropriate rotation of the north-south, east-west horizontal SRO recordings. Note the pronounced dependence of the phase of SS upon the source-receiver azimuth not previously noticed in the P-wave data.

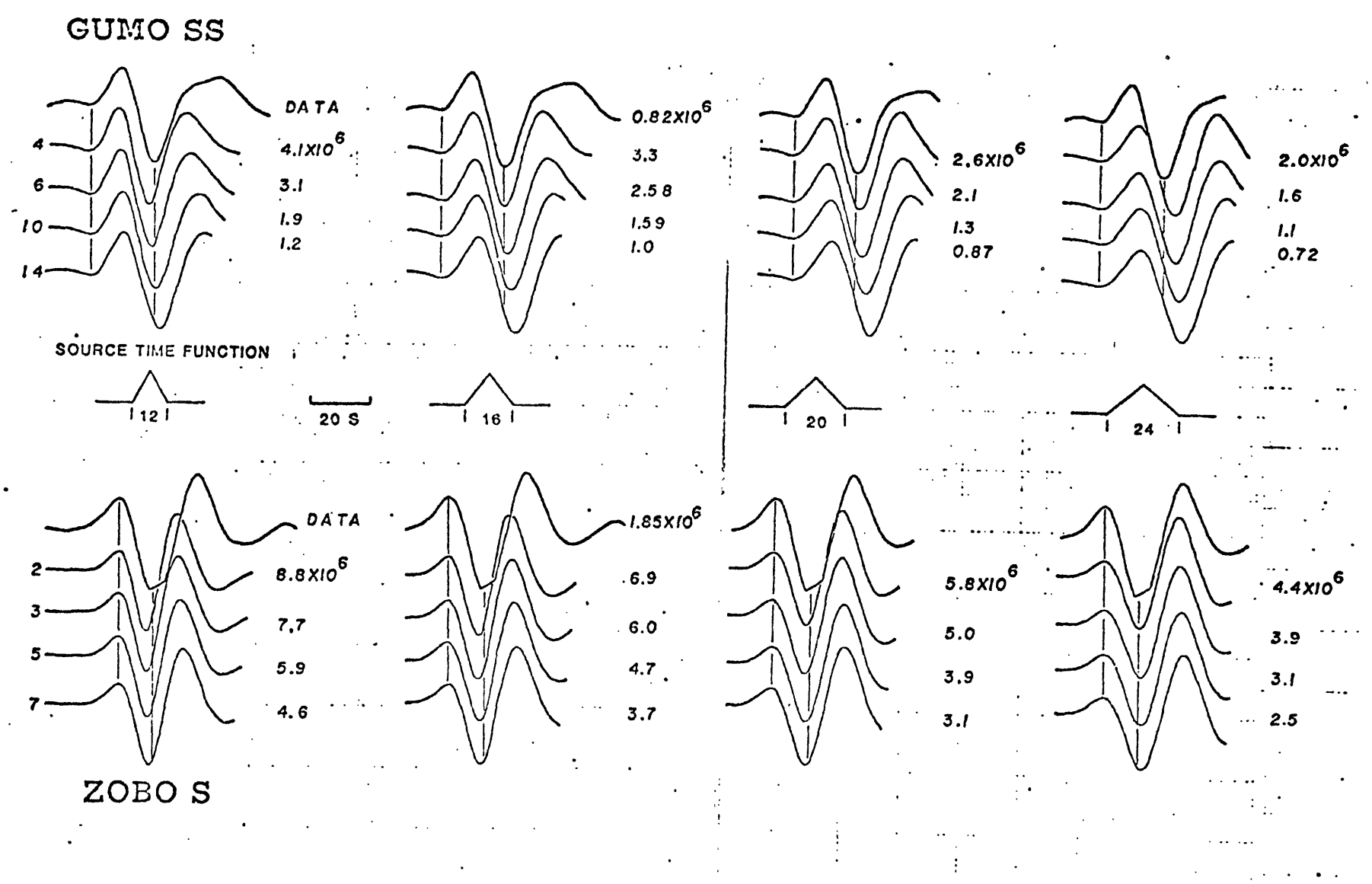

Figure 8. GUMO SS and ZOBO S data compared with synthetics assuming various values of t* shown at the left and different lengths of the source-time function shown along the center. No single source time length-t* combination is consistent with both data. In all cases, the predicted amplitudes are much too large assuming a source moment of 3×10^{27} dyne-cm.

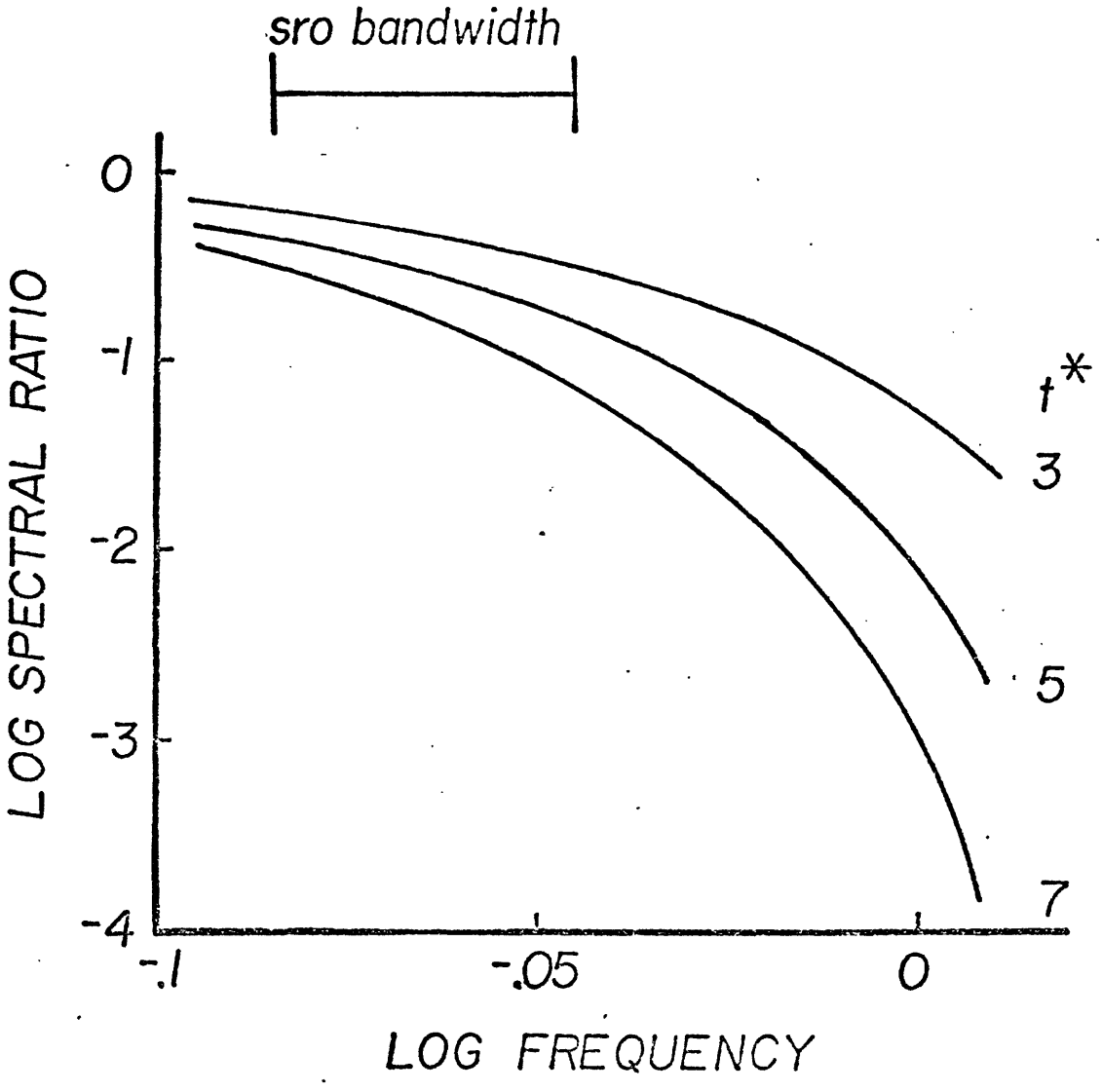

Figure 9. Amplitude spectra of the attenuation operator for t* values of 3, 5 and 7. The SRO bandwidth is approximated at the top. Obviously, any reasonable choice of t* will have little effect on the predicted amplitudes.

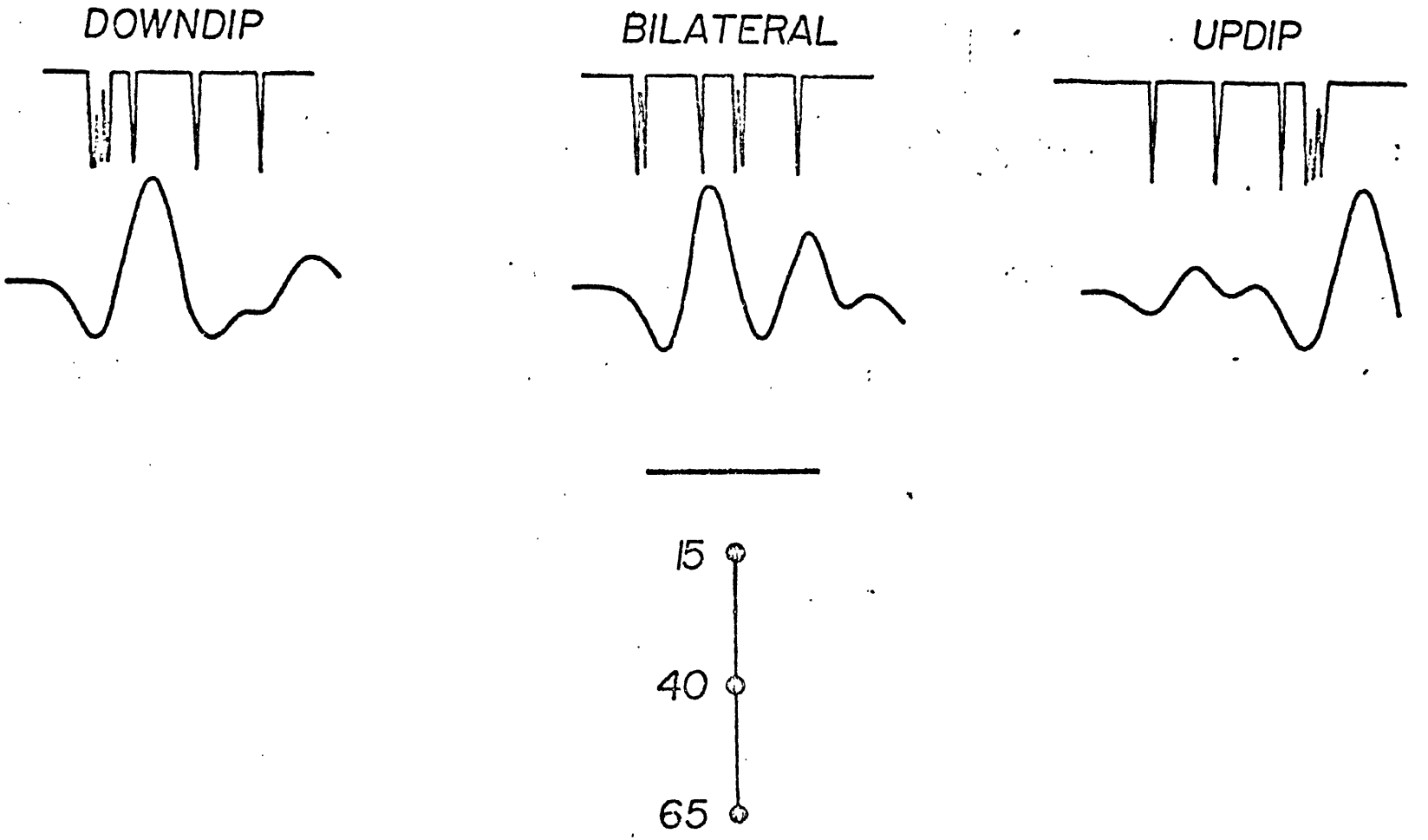

Figure 10. Synthetic seismograms for a vertical, linear fault with three discrete sources. Updip propagation yields a maximum delay wavelet, while downdip propagation produces the opposite effect. The Green's functions are plotted in the top of each frame while the bottom frame has been convolved with the SRO impulse response. The seismograms are tangential responses at an epicentral distance of 60°.

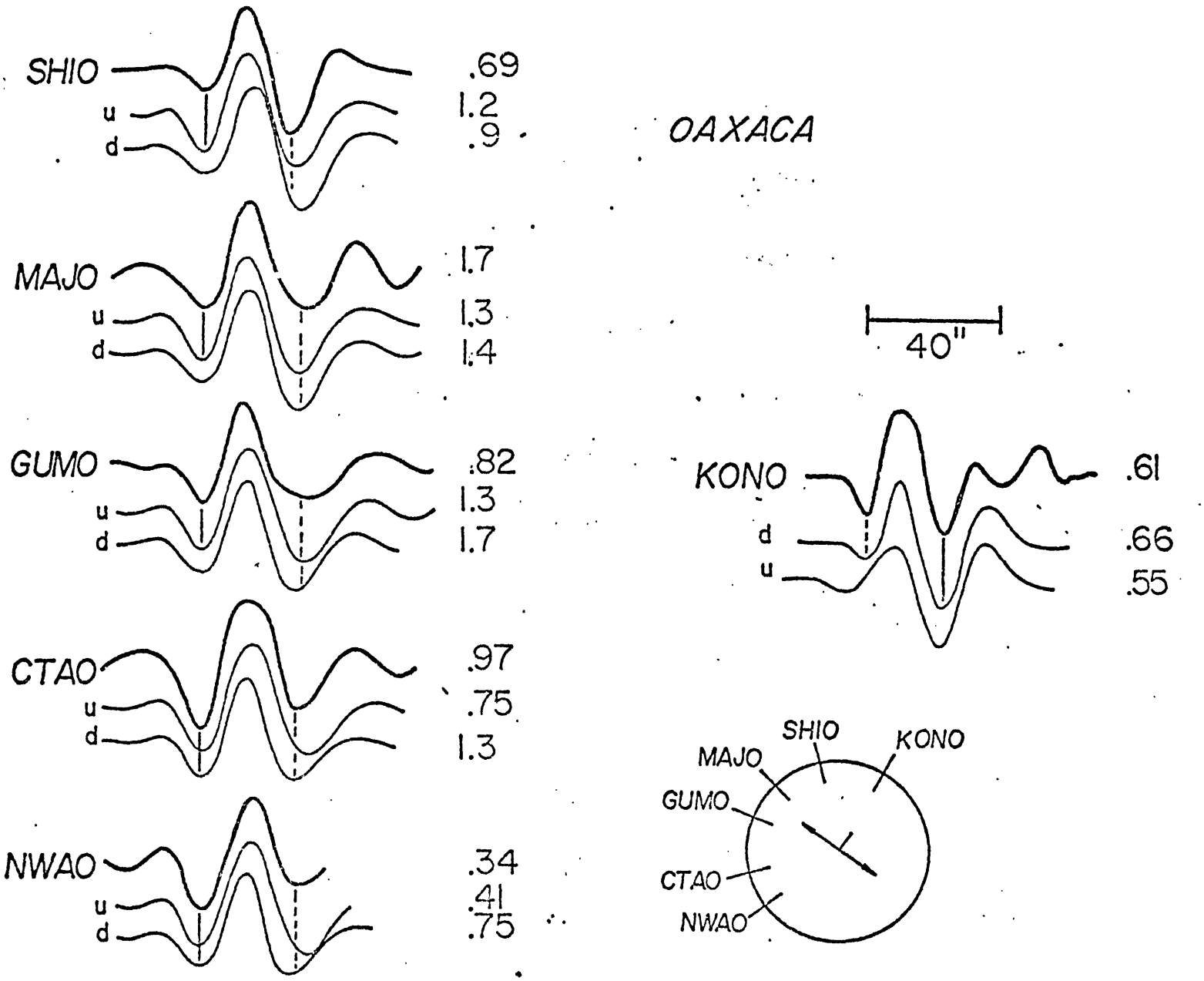

Figure 11. Synthetic seismograms for the various S-wave data assuming a 90 km long fault with bilateral propagation to each side to a range of 30 km. "d" denotes downdip, while "u" signifies updip propagation. In general, downdip propagation fits the phase and amplitude data best. The azimuthal dependence of the phase is properly modeled by the synthetics.

REFERENCES FOR APPENDIX A

Chapman, C. H., (1978). A new method for computing synthetic seismograms. Geophys. J. Roy. Astr. Soc., 54, 481 - 518.

Futterman, W. I., (1962). Dispersive body waves. J. Geophys. Res., 67, 5279 - 5291.

Reyes, A., J. N. Brune and Cinna Lomnitz, (1979). Source mechanism and aftershock study of the Colima, Mexico earthquake of January 10, 1973. Bull. Seismo. Soc. Am., 69, 1819 - 1840.

Minster, J. R. and T. H. Jordan, (1978). Present-day plate motions. J. Geophys. Res., 83, 5331 - 5354.

Singh, S. K., J. Havskov, K. C. McNally, L. Ponce, T. Hearn and M. Vassiliov, (1980). The Oaxaca, Mexico earthquake of 29 November 1978: a preliminary report on aftershocks. Science, 207, 1211 - 1213.

Reyes, A., J. Gonzalez, L. Munguia, A. Nava, F. Vernon and J. N. Brune, (1978). Locations of aftershocks of the Oaxaca earthquake using smoked paper recorders and digital event recorders. Geofisica Internacional, 17, 341 - 350.